Cellular/Molecular

Oxidative Phosphorylation, Not Glycolysis, Powers Presynaptic and Postsynaptic Mechanisms Underlying Brain Information Processing

Catherine N. Hall, Miriam C. Klein-Flügge, Clare Howarth, and David Attwell
Department of Neuroscience, Physiology and Pharmacology, University College London, London WC1E 6BT, United Kingdom

Neural activity has been suggested to initially trigger ATP production by glycolysis, rather than oxidative phosphorylation, for three reasons: glycolytic enzymes are associated with ion pumps; neurons may increase their energy supply by activating glycolysis in astrocytes to generate lactate; and activity increases glucose uptake more than O_2 uptake. In rat hippocampal slices, neuronal activity rapidly decreased the levels of extracellular O_2 and intracellular NADH (reduced nicotinamide adenine dinucleotide), even with lactate dehydrogenase blocked to prevent lactate generation, or with only 20% superfused O_2 to mimic physiological O_2 levels. Pharmacological analysis revealed an energy budget in which 11% of O_2 use was on presynaptic action potentials, 17% was on presynaptic Ca^{2+} entry and transmitter release, 46% was on postsynaptic glutamate receptors, and 26% was on postsynaptic action potentials, in approximate accord with theoretical brain energy budgets. Thus, the major mechanisms mediating brain information processing are all initially powered by oxidative phosphorylation, and an astrocyte–neuron lactate shuttle is not needed for this to occur.

Introduction

Brain function depends critically on an adequate energy supply, in the form of oxygen and glucose provided in the blood, which is largely used on reversing the ion influxes underlying synaptic potentials and action potentials (Attwell and Laughlin, 2001). Averaged over time, brain ATP is almost entirely generated by the complete oxidation of glucose: glycolysis followed by oxidative phosphorylation results in a ratio of oxygen to glucose consumption of ~6:1, and oxidative phosphorylation provides ~87% (26 of 30 molecules) of the ATP generated (Kety, 1957; Sokoloff, 1960). In the short term, however, when neuronal activity increases, ATP has been suggested to be initially produced by glycolysis, for three reasons.

First, both in brain and other tissues, glycolytic membrane-bound enzymes are directly associated with ion pumps such as the Na^+/K^+-ATPase (Knull, 1978; Paul et al., 1979; Mercer and Dunham, 1981; Lipton and Robacker, 1983; Dubinsky et al., 1998), H^+-ATPase (Lu et al., 2001), and Ca^{2+}-ATPase (Paul et al., 1989), suggesting that ion transport may be fuelled by ATP produced in a local compartment by glycolysis (Mercer and Dunham, 1981). Second, it has been proposed that neurons regulate their energy supply by turning on glycolysis in astrocytes. When active neurons release glutamate it is taken up into astrocytes, which are proposed to use glycolytically derived ATP to power this uptake and the subsequent conversion of glutamate to glutamine, thus producing lactate which is exported to neurons as a substrate for mitochondrial oxidative phosphorylation (Pellerin and Magistretti, 1994; Magistretti et al., 1999). Third, because the increase in oxygen uptake during neural activity was found to be disproportionally small compared to the increase in blood flow and glucose uptake, it was suggested that glycolysis is the main energy-providing mechanism initially supporting neural activity (Fox et al., 1988). The fact that O_2 uptake is small relative to the blood flow increase is the basis of BOLD functional imaging (Ogawa et al., 1993).

The notion that neuronal activity initially increases glycolytic ATP production, often assumed to be in astrocytes with subsequent transfer of lactate to neurons for oxidative phosphorylation, has become established in the literature (Hyder et al., 2006; Pellerin et al., 2007; Barros and Deitmer, 2010). However, this concept is based on techniques that have a relatively poor temporal resolution and has been challenged by the demonstration that activity evokes a decrease in extracellular oxygen concentration (Malonek and Grinvald, 1996; Thompson et al., 2003) and a decrease in intracellular NADH (reduced nicotinamide adenine dinucleotide) (Kasischke et al., 2004; Brennan et al., 2006), both of which are consistent with at least some ATP being generated by oxidative phosphorylation.

We demonstrate that oxidative phosphorylation is the main mechanism initially providing energy to power neuronal activity, that the main subcellular mechanisms underlying information processing, i.e., presynaptic action potentials, neurotransmitter release, postsynaptic currents, and postsynaptic action potentials, all consume oxygen, and that an astrocyte–neuron lactate shuttle is not needed for oxidative phosphorylation to occur.

Received Jan. 3, 2012; revised April 20, 2012; accepted May 9, 2012.

Author contributions: C.N.H., M.C.K.-F., C.H., and D.A. designed research; C.N.H., M.C.K.-F., C.H., and D.A. performed research; C.N.H., M.C.K.-F., C.H., and D.A. analyzed data; C.N.H., M.C.K.-F., C.H., and D.A. wrote the paper.

This work was supported by the European Research Council, Fondation Leducq, and the Wellcome Trust. We thank Paikan Marcaggi and Marieke Schölvinck for early work on this project.

Correspondence should be addressed to David Attwell at the above address. E-mail: d.attwell@ucl.ac.uk.

DOI:10.1523/JNEUROSCI.0026-12.2012

 0270-6474/12/328940-12$15.00/0

Materials and Methods

Brain slices. Coronal brain slices (300 μm thick) containing the hippocampus were prepared on a vibratome from postnatal day 21 (P21) Sprague Dawley rats (of either sex), killed by cervical dislocation in accordance with UK government regulations. Slices were incubated for 30 min at 37°C, and then for at least 30 min at room temperature in oxygenated (95% O_2/5% CO_2) artificial CSF (ACSF) containing the following (in mM): 124 NaCl, 2.5 KCl, 26 $NaHCO_3$, 1 $MgCl_2$, 1 NaH_2PO_4, 10 glucose, 2 $CaCl_2$, and 1 kynurenic acid (to block glutamate receptors).

Experimental solutions. Slices were perfused with bicarbonate-buffered ACSF, as described above, but without the kynurenic acid, at 35°C. In experiments using 20% oxygen, the perfusion solution was bicarbonate-buffered ACSF, gassed with 20% O_2, 5% CO_2, and 75% N_2.

Recording field potentials. Synaptic and action potential activity was evoked by stimulating the Schaffer collaterals in the stratum radiatum of area CA3 with a concentric bipolar tungsten electrode while monitoring the field potential in the stratum pyramidale in CA1, using a glass microelectrode filled with ACSF (see Fig. 1*A*). Field potentials were measured with a patch clamp, as the current needed to hold the electrode at 0 mV. Consequently, they have a current amplitude given by the voltage deflection occurring in the extracellular space divided by the resistance of the electrode (~2 MΩ) and are inverted in sign compared to voltage recordings. Each stimulus was 60 μs long, 50–90 V, and delivered at 0.33 Hz (to monitor the effects of drugs on different components of the field potential) or at 20 Hz (when evoking sufficient neuronal activity to detect changes in extracellular [O_2]). Field potentials were analyzed, as in Figure 1*B*, to provide a measure of the presynaptic action potential volley (proportional to the number of fibers excited), the postsynaptic field potential (fEPSP, proportional to the product of the number of fibers excited and the EPSC evoked in each postsynaptic cell), and the postsynaptic action potential (population spike, determined by the number of postsynaptic cells that fire action potentials in response to the synaptic input).

O_2 electrode recordings. Extracellular O_2 levels were measured using a glass Clark type oxygen microelectrode with a 10 μm tip (Unisense), which was inserted ~100 μm into the slice, with its tip center in the stratum radiatum 30 μm from the pyramidal cell layer (Fig. 1*A*). The electrode was calibrated at least once a week using distilled water at 35°C equilibrated with 0, 20, and 100% oxygen. Oxygen electrode and field potential recordings were acquired using pClamp 10.1 (Molecular Devices), which was also used to control the stimulation. The O_2 concentration in the bulk solution entering the bath was 543 ± 15 μM ($n = 3$), i.e., lower than the ~1 mM in the solution bubbled with 95% O_2/5% CO_2 because of O_2 loss through the plastic walls of the tube connecting the solution reservoir to the bath.

NADH imaging. Reduced NADH is fluorescent (Aubin, 1979), while its oxidized form NAD^+ is not. Reduced NADH in area CA1 of the hippocampus (including the strata radiatum, pyramidale and oriens; see Fig. 1*A*) was imaged by focusing just below the slice surface using bright-field microscopy with a 20× or 40× water-immersion objective. NADH fluorescence was excited using a xenon arc lamp, with a 300–370 nm excitation filter, 420–490 nm emission filter, and 410 nm dichroic filter. Emitted light was imaged using a CoolSnapHQ^2 CCD camera and ImagePro software (Media Cybernetics), with an exposure time of 2 s and a capture rate of 0.41 Hz. Images were analyzed with ImageJ software.

Experimental protocol. For most experiments NADH images, field potential recordings, and [O_2] measurements were obtained simultaneously. The standard protocol (Fig. 2*A*) consisted of two phases: 30 s of 0.33 Hz stimulation followed (after 30 s with no stimulation) by 10 s of stimulation at 20 Hz to generate an easily detectable metabolic response in the tissue (no stimulation was applied after this). The frequency of 20 Hz is similar to the peak firing rate produced in CA3 cells *in vivo* for optimal stimuli (mean value of 13 Hz, but extending up to 25 Hz) (Leutgeb et al., 2007).

This protocol was then repeated three times at an interval of 6 min for each drug condition, and the field potential, O_2, and NADH results from each triplicate were averaged. The first triplicate in each slice was drug free and was used as a control to which later triplicates were normalized. Since responses might change with time even under control conditions, to assess the effect of drugs we first assessed whether the response to a second control triplicate differed significantly from the first triplicate, and, if it did, we compared the mean response in the second triplicate performed in the presence of drug with the mean response in the second triplicate performed in the absence of drug. For most experiments (including all from which the field potential was analyzed), 1 μM TTX was added for the final stimulation triplicate. TTX abolishes all components of the field potential leaving only the stimulation artifact (Fig. 1*B*), which was subtracted from the previous recordings from the same slice to reveal the various field potential components.

Lactate measurements. To assess the effect of the lactate dehydrogenase (LDH) inhibitor oxamate on hippocampal slice lactate levels, slices were incubated in 1 ml ACSF with and without 20 mM oxamate at 37°C for 5 min (the earliest time at which measurements were taken after incubating slices with oxamate in the stimulation experiments). The slices were then removed, and the bathing solution was assayed for lactate content using a commercially available colorimetric assay based on the reaction of lactate oxidase (Abcam; some other lactate sensors are based on lactate dehydrogenase which would be inappropriate for experiments attempting to block this enzyme in the cells). This gave an absorbance proportional to lactate concentration over the range 0 to 10 mM, and the lactate concentration in the bathing ACSF was determined by comparison to known lactate concentrations. Oxamate (20 mM) did not affect the slope or intercept of the graph of absorbance as a function of concentration (slope increased by 3.6%, $p = 0.87$; intercept increased by 1%, $p = 0.93$), implying that oxamate did not inhibit the assay lactate oxidase.

Statistics. Statistical analysis was conducted using SPSS 16 or the StatTools resources (http://department.obg.cuhk.edu.hk/researchsupport/statmenu.asp). Unless stated otherwise, Student's two-tailed t test was used. Where multiple comparisons are presented, p values were corrected using a procedure equivalent to the Holm–Bonferroni method (for N comparisons, the most significant p value is multiplied by N, the second most significant by $N - 1$, the third most significant by $N - 2$, etc.; corrected p values are significant if they are <0.05). Data are presented as mean ± SEM.

Results

Experimental approach

In this paper we use hippocampal slices to assess how energy is provided in response to stimulated activity by combining oxygen electrode recording, NADH imaging, and modeling of how O_2 concentration changes relate to O_2 consumption. The slice preparation is crucial for these experiments for three reasons. First, unlike for cultured cells, the spatial relationship of neurons and astrocytes is preserved. Second, it allows pharmacological agents to be applied at a defined concentration. Third, and most importantly, unlike in intact brain, oxygen is supplied to the slice by diffusion from the perfusing solution, so that changes in the oxygen concentration in the slice reflect only changes in the rate of oxygen use and do not require complex modeling to interpret (Gjedde, 2005). This is critically different from the *in vivo* brain, where the amount of oxygen supplied by the blood is often altered by the same experimental manipulations that alter oxygen use, confounding the interpretation of experiments. For example, glutamate receptor antagonists and inhibition of lactate production, as used below, will decrease blood flow (Brazitikos et al., 1993; Akgören et al., 1994; Li and Iadecola, 1994; Gordon et al., 2008), reducing oxygen supply (Offenhauser et al., 2005) and confounding the quantification of any effect on oxygen consumption.

Neuronal activity lowers extracellular O_2 and intracellular NADH levels

Figure 1, *A* and *B*, shows the experimental arrangement and typical field potentials recorded when stimulating the Schaffer collaterals at 0.33 Hz, including a small and brief presynaptic action potential volley, the field EPSP (a downward deflection when

measured as a current, lasting about 15 ms), and the population spike (a brief upward deflection reflecting the occurrence of postsynaptic action potentials).

On advancing the oxygen electrode from the bulk perfusion solution to a position ~100 μm below the surface of the slice, the O_2 level decreased from the bulk solution value of 543 μM (see Materials and Methods) to a mean value of 212 ± 17 μM in 86 slices. A 10 s train of stimulation at 20 Hz produced a decrease of O_2 level of 118 ± 8 μM in 86 slices (Fig. 1*C*, specimen trace). At the same time there was a 1.4 ± 0.2% initial decrease in NADH fluorescence (averaged over the CA1 region), followed by a 2.4 ± 0.3% increase above the original level (in 26 slices; Fig. 1*D*, specimen trace). In the stratum oriens, the resting NADH fluorescence was a little lower than in the strata pyramidale or radiatum (Fig. 1*E*), but neither the initial decrease of NADH level evoked by stimulation (Fig. 1*F*) nor the overshoot of [NADH] after stimulation (Fig. 1*G*) differed significantly between the three layers.

The decrease of $[O_2]$ implies that the rate of ATP production by oxidative phosphorylation has been increased. This may be due to ATP consumption leading to a rise in the [ADP]/[ATP]ratio (Chance and Williams, 1955), due to a rise of mitochondrial $[Ca^{2+}]$ activating the F_0F_1-ATPase (Territo et al., 2000) (but see Gellerich et al., 2010), or due to a rise of extramitochondrial $[Ca^{2+}]_i$ activating the mitochondrial aspartate–glutamate exchanger aralar (Contreras and Satrústegui, 2009; Gellerich et al., 2009), which raises [NADH] in mitochondria and thus supports H^+ pumping out across the mitochondrial membrane. We will show below that the majority of the ATP produced in response to neuronal activity is by oxidative phosphorylation. The fall of NADH level is expected if neuronal activity increases oxidative phosphorylation to a rate that consumes NADH faster than it can be provided by the tricarboxylic acid (TCA) cycle and glycolysis (Fig. 1*H*). The subsequent overshoot in [NADH] to a value higher than the original level may reflect a late activation of glycolysis in astrocytes or neurons (Kasischke et al., 2004) as is sometimes assumed, but could alternatively be due to increased NADH production by the TCA cycle (Brennan et al., 2006) occurring when a rise of mitochondrial $[Ca^{2+}]_i$ activates mitochondrial dehydrogenases (Duchen, 1992) (for review, see Gunter et al., 2004; Gellerich et al., 2010) (but see Mathiesen et al., 2011).

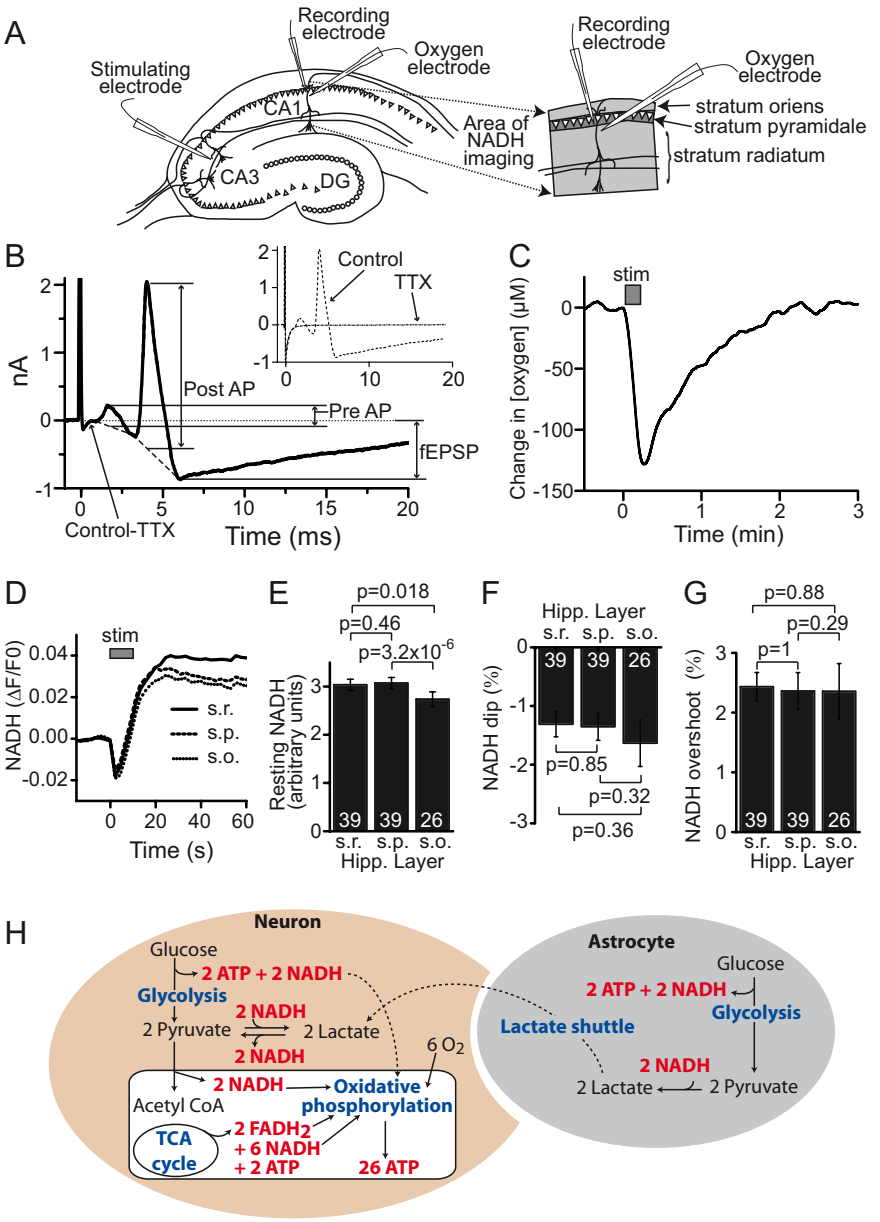

Figure 1. Stimulus-evoked field potentials and O_2 and NADH changes. ***A***, Diagram of the electrode positions and area imaged. ***B***, Inset: Specimen field potentials evoked at 0.33 Hz, in the absence and presence of TTX. Main panel: Trace from inset without TTX minus the trace in TTX, annotated to show how field potential amplitudes were measured. ***C***, Decrease of extracellular $[O_2]$ evoked by 10 s of 20 Hz stimulation. ***D***, Biphasic NADH response (change in fluorescence/fluorescence at the start of stimulation, $\Delta F/F0$) evoked by 10 s of 20 Hz stimulation in the stratum radiatum (s.r.), stratum pyramidale (s.p.), and stratum oriens (s.o.). ***E–G***, Resting NADH fluorescence (***E***), decrease of NADH fluorescence evoked by 20 Hz stimulation (***F***), and subsequent increase of NADH fluorescence above resting level (***G***) in the s.r., s.p., and s.o. All *p* values are from paired *t* tests. ***H***, How the rates of glycolysis, the TCA cycle, and oxidative phosphorylation determine whether the NADH level falls or rises. An increase in the rate of oxidative phosphorylation will lower [NADH]. An increase in the rate of glycolysis (in astrocytes or in neurons) will increase [NADH], if not balanced by NADH consumption in the conversion of pyruvate to lactate, as will an increase in the rate of the tricarboxylic acid cycle. Lactate dehydrogenase is proposed to convert pyruvate to lactate in astrocytes, and lactate to pyruvate in neurons.

O_2 use on different subcellular mechanisms

The main energy-demanding processes mediating information processing, i.e., presynaptic action potentials, transmitter release, postsynaptic currents, and postsynaptic action potentials (Attwell and Laughlin, 2001), occur in different subcellular compartments, and thus may differ in their dependence on ATP generation by glycolysis and oxidative phosphorylation. To assess this, we applied drugs to block, successively, postsynaptic currents and postsynaptic action potentials [10 μM NBQX and 50 μM D-AP5 (NBQX+AP5)], presynaptic transmitter release and downstream postsynaptic events (250 μM Cd^{2+}), and finally all action potentials and synaptic events (1 μM TTX).

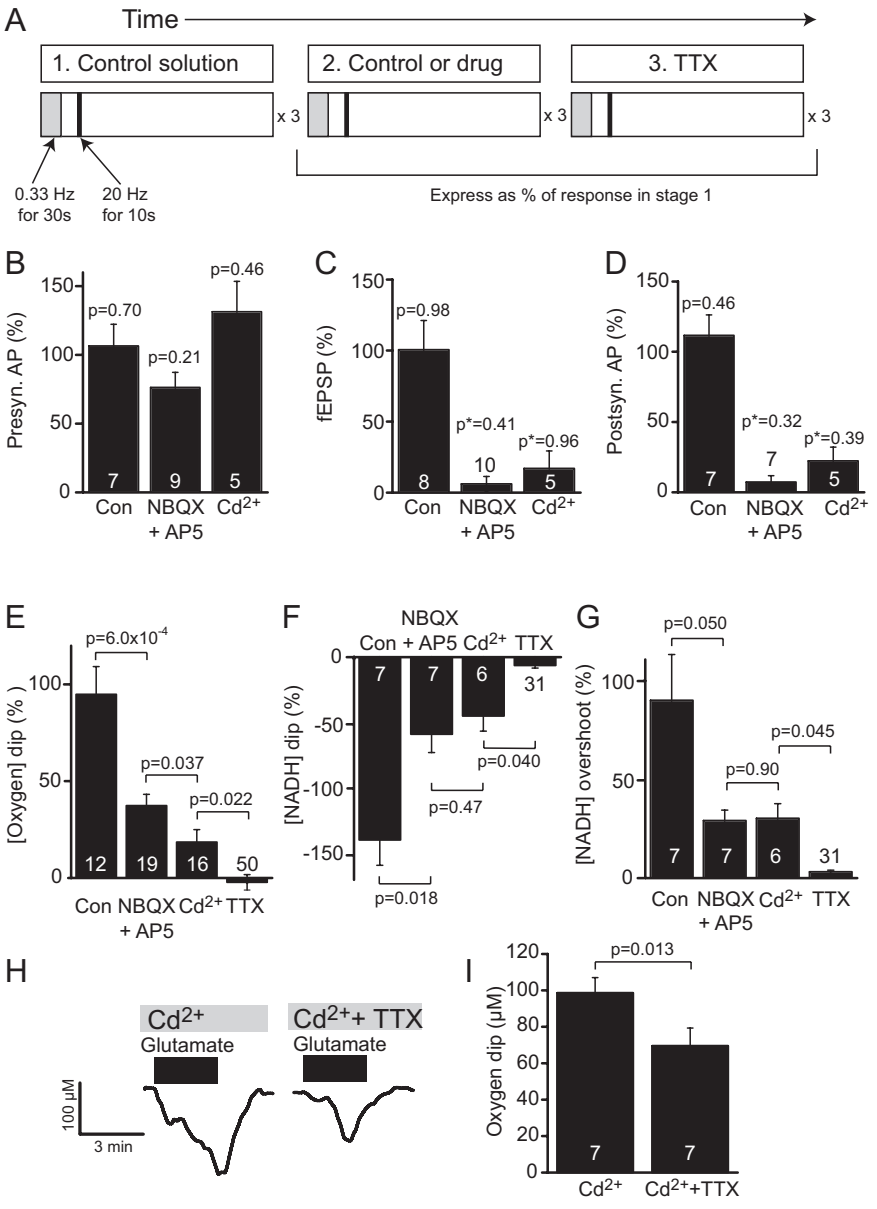

Figure 2. Pharmacological analysis of O_2 use on different subcellular mechanisms. ***A***, Schematic showing experimental protocol, with three stimulation sets in each condition applied at 6 min intervals (see Materials and Methods): during the first stimulation phase, no drug is present for all slices. In the second phase, some slices are exposed to drug, while some remain drug free as controls. In the third phase, 1 μM TTX is applied (to allow subtraction of the stimulation artifact from the field potential data). Responses in phase 2 are reported as a percentage of the response in phase 1, to normalize to the number of axons activated in each slice. Comparing the normalized responses for control and drug in phase 2 defines the effect of the drug tested. ***B–D***, Amplitude of presynaptic action potential volley (***B***), postsynaptic field EPSP (***C***), and postsynaptic action potential population spike (***D***) measured as in Figure 1*B*, in the presence of NBQX+AP5 or Cd^{2+} together with the amplitude seen on the second application of 20 Hz stimulation in the absence of drugs (Con). The *p* values are from one sample *t* tests comparing with 100% (the response in the first stimulation phase), unless marked with an asterisk, in which case the comparison is versus zero. ***E–G***, Amplitude of the $[O_2]$ decrease (***E***), decrease in NADH fluorescence (***F***), and overshoot of NADH fluorescence above its baseline value (***G***) in the presence of NBQX+AP5, Cd^{2+}, and TTX, compared to the amplitude seen on the second application of 20 Hz stimulation in the absence of drugs (Con; these values are not significantly different from the responses to the first set of stimuli). Incrementally blocking postsynaptic activity (NBQX+AP5), transmitter release (Cd^{2+}), and all evoked activity (TTX) incrementally decreased the $[O_2]$ decrease. The *p* values are from unpaired *t* tests, corrected for multiple comparisons. ***H***, ***I***, Specimen traces (***H***) and mean values (***I***) for the decrease of $[O_2]$ evoked by 500 μM glutamate in 250 μM Cd^{2+} and in Cd^{2+} + 1 μM TTX. The resting $[O_2]$ was not significantly affected by Cd^{2+} (reduced by 42 ± 36%; $p = 0.29$) nor by TTX (in Cd^{2+}; reduced by 12 ± 36%; $p = 0.75$) in seven slices.

To assess the effects of the drugs used, we analyzed the extracellular field potentials. As expected, postsynaptic currents and postsynaptic action potentials were selectively abolished by NBQX+AP5, with no significant effect on the presynaptic action potential (Fig. 2*A–D*). Cd^{2+} also abolished postsynaptic events but spared the presynaptic action potential, while TTX abolished all electrical activity (Fig. 1*B*). We also tried using muscimol (20 μM) to activate $GABA_A$ receptors and thus prevent the postsynaptic cells from firing action potentials (Caesar et al., 2003), in an attempt to define the O_2 use on postsynaptic action potentials. However, as observed by Jang et al. (2005), high levels of muscimol reduced the field EPSP by ~40% (data not shown), suggesting that presynaptic $GABA_A$ receptors reduce transmitter release, which would have confounded our allocation of O_2 consumption to different subcellular mechanisms.

Blocking postsynaptic currents, and the postsynaptic action potentials they produce, with NBQX+AP5 reduced the 20 Hz stimulation evoked decrease of O_2 level by 63% ($p = 2.7 \times 10^{-9}$, compared to the preceding responses in the absence of drugs). The response in NBQX+AP5 was significantly smaller than the O_2 response to a second set of stimulation in the absence of any drug ($p = 6 \times 10^{-4}$, Fig. 2*E*), while applying the stimulation twice with no drug application had no significant effect on the O_2 decrease ($p = 0.73$; Fig. 2*E*, Con). Applying Cd^{2+}, to additionally block presynaptic processes controlling transmitter release downstream of Ca^{2+} entry as well as all processes (in addition to postsynaptic currents) activated by transmitter release [such as uptake and metabolic processing of transmitter, and activation of metabotropic glutamate receptors (mGluRs)], reduced the O_2 decrease by an additional 19% (Fig. 2*E*), while TTX abolished the O_2 decrease. A similar series of reductions of the NADH fluorescence decrease (Fig. 2*F*), and overshoot (Fig. 2*G*) was seen when these drugs were applied. The NADH changes seen on drug application were not significantly different across the layers of the hippocampus (repeated-measures ANOVA, $p = 0.42$), so for this and subsequent experiments NADH data were averaged across the whole CA1 region.

These data indicate that oxidative phosphorylation is used to generate at least some of the ATP used to power presynaptic action potentials, presynaptic processes controlling transmitter release, and postsynaptic currents and action potentials.

Separating postsynaptic O_2 use on glutamate-gated currents and action potentials

Calculations presented below show that the 63% reduction of the $[O_2]$ decrease produced by NBQX+AP5 implies that 72% of the

O_2 is used postsynaptically. However, this does not distinguish O_2 use on postsynaptic glutamate receptor currents and on postsynaptic action potentials. To determine whether both or just one of these processes is powered by ATP from oxidative phosphorylation, we applied glutamate (500 μM) to activate AMPA/KA, NMDA, and metabotropic glutamate receptors, and thus to generate action potentials (the glutamate level reached deep in the slice will be in the low micromolar range because of uptake) (Amato et al., 1994). The experiments were performed in the presence of 250 μM Cd^{2+} to prevent the evoked action potentials from releasing more neurotransmitter. Repeated application of glutamate (in Cd^{2+}) evoked an [O_2] decrease that was not significantly different on the second application ($p = 0.93$; Fig. 2*I*, Cd^{2+}), while if TTX was present during the second glutamate application (to block glutamate-evoked action potentials but not Na^+ entry through glutamate-gated channels), the O_2 decrease was reduced by 29% ($p = 0.013$; $n = 7$; Fig. 2*H*,*I*), reflecting the suppression of O_2 use on reversing the ion movements associated with action potentials.

The dependence of action potential firing rate on mean glutamate-gated current, and hence the relative magnitudes of the ion influxes through glutamate-gated channels and through voltage-gated Na^+ channels, may differ when action potentials are evoked by superfusing glutamate (as here) and by activating the Schaffer collateral input (as in Fig. 2*E*). In addition, superfusion of glutamate may activate extrasynaptic and astrocyte receptors that are not activated by synaptic glutamate release. However, the data in Figure 2, *H* and *I*, demonstrate that activation of glutamate receptors, and the action potentials this produces, both evoke O_2 use on ATP production by oxidative phosphorylation.

Oxidative phosphorylation is evoked by neuronal activity at physiological O_2 levels

The experiments described above used, as is customary, 95% oxygen (~1 mM) in the superfusion solution, which leads to an oxygen level in the brain slices of ~150–400 μM (at different depths in the slice) (see Fig. 6*A*,*B*), which is much higher than the *in vivo* value of 20–60 μM (Dings et al., 1998; Offenhauser et al., 2005). The fraction of ATP which is produced by oxidative phosphorylation might be reduced by the lower *in vivo* value, which can be mimicked by superfusing brain slices with solution equilibrated with 20% oxygen (Hall and Attwell, 2008), giving an oxygen level of 2–130 μM at different depths in the slice (data not shown). We therefore investigated the changes of O_2 level and NADH fluorescence produced by neuronal activity in slices superfused with solution containing 20% O_2.

Switching from 95% to 20% O_2 in the superfusion solution did not significantly affect the amplitude of the presynaptic action potential ($p = 0.24$), though the postsynaptic fEPSP (38% decrease; $p = 1.3 \times 10^{-4}$) and the postsynaptic population spike (15% decrease; $p = 0.014$; Fig. 3*A*) were significantly reduced. This reduction in postsynaptic responses may reflect a rise in the adenosine concentration in the slice in the lower O_2 solution (Gordon et al., 2008), which acts on presynaptic receptors to reduce glutamate release. As was shown in Figure 2*B–D* for 95% O_2, NBQX+AP5 abolished the fEPSP and population spike, with no effect on the presynaptic action potential, while TTX abolished all evoked electrical activity (n = 5–6 slices) (data not shown).

In 20% O_2, the resting O_2 level before stimulation was 115 ± 25 μM ($n = 18$), i.e., only 54% of the value measured with 95% O_2 in the superfusion solution. Thus, there is less O_2 available to be consumed during periods of increased energy demand, and stimulation of the Schaffer collaterals could not lower the [O_2] by the same amount as occurs in 95% O_2 solution (~120 μM; Fig. 1). Accordingly, the initial decrease in [O_2] was only 22 ± 3% of that seen in 95% O_2 solution, but the time course of the dip was significantly prolonged (Fig. 3*B*,*D*; it recovered to baseline in ~5 min), consistent with ion pumping being powered by oxidative phosphorylation for a longer period after neuronal activity in 20% O_2. Similarly, the initial decrease and late overshoot of NADH fluorescence averaged over the CA1 area were also reduced in 20% O_2 solution (Fig. 3*C*). Switching from 95% to 20% O_2 solution increased the resting NADH fluorescence by 5 ± 2% ($p = 0.018$; $n = 15$). The time courses of the [O_2] and [NADH] changes are compared in Figure 3*D*. At both superfused O_2 levels, the overshoot of the NADH concentration overlaps with much of the period of increased O_2 use.

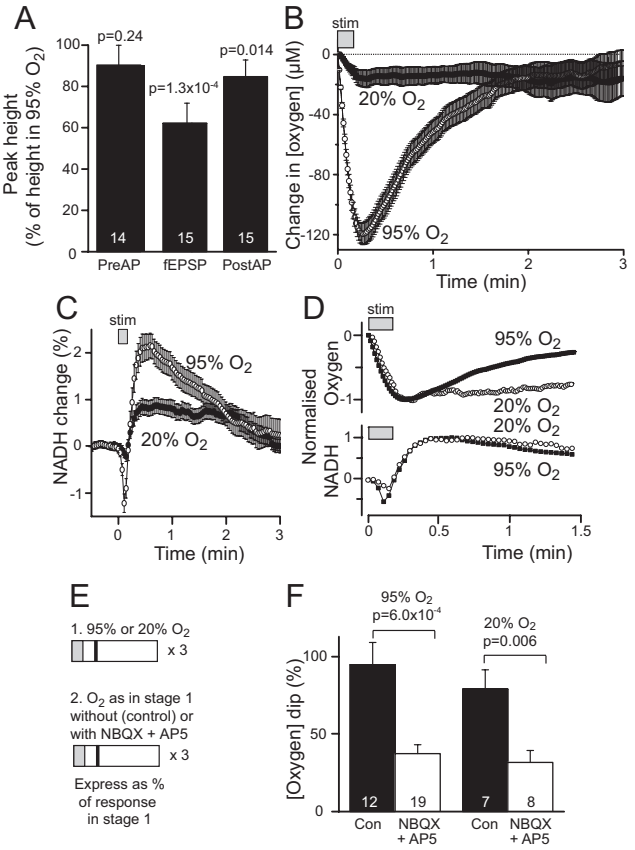

Figure 3. Oxidative phosphorylation powers neuronal activity at physiological [O_2]. ***A***, Effect of switching from 95% to 20% O_2 in the superfusion solution on the amplitude of the presynaptic action potential, the postsynaptic fEPSP, and the postsynaptic action potential (population spike). ***B***, Mean time course of [O_2] decrease in 20% O_2 solution in 15 slices, compared with that in 95% O_2 solution (56 slices). ***C***, Mean time course of NADH changes in 20% and 95% O_2 solution (in 11 and 15 slices, respectively). ***D***, Oxygen and NADH responses in 20% (open circles) and 95% (filled squares) O_2, normalized to the peak dip and overshoot, respectively. ***E***, ***F***, Effect of GluR blockers on O_2 dip in 95% and 20% O_2. ***E***, Experimental design. The first stimuli were presented in 95% or 20% O_2. The same [O_2] was maintained for the second stage, when NBQX+AP5 was applied to 8 of 15 slices in 20% O_2 or 19 of 31 slices in 95% O_2. ***F***, Effect of NBQX+AP5 on the oxygen dip in 95% and 20% O_2. Control bars show response to second stimulation normalized to response to first stimulation in the same O_2 (not significantly different from the response to the first stimulation, $p = 0.73$ for 95%; 0.14 for 20% O_2). NBQX+AP5 bars show response to second stimulation in NBQX+AP5 normalized to response to first stimulation without drugs in the same O_2. There was no significant difference between the effect of NBQX+AP5 in the two O_2 concentrations (univariate ANOVA, $p = 0.64$).

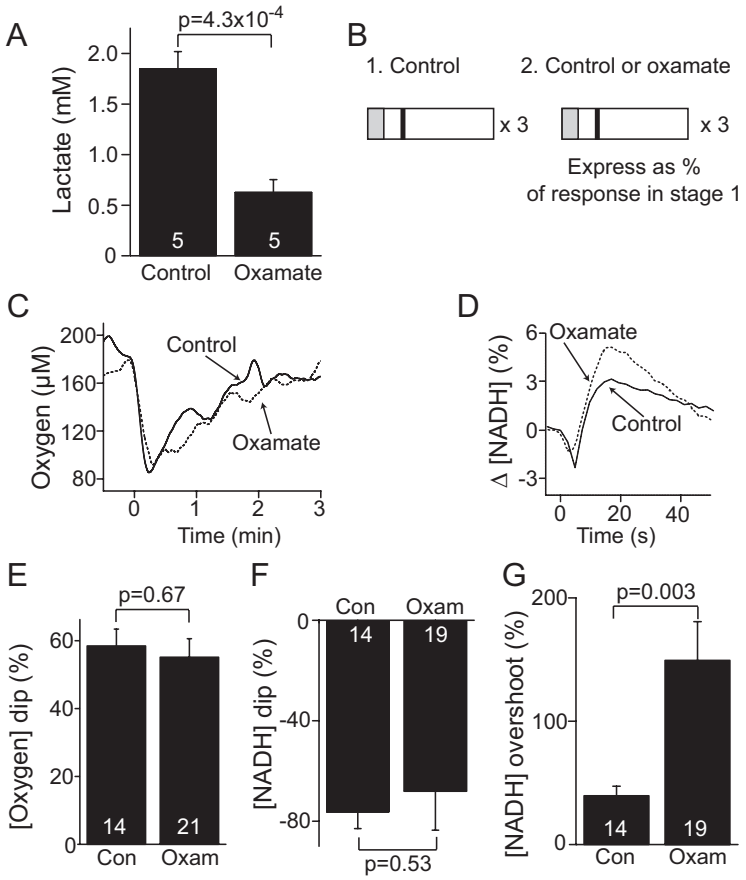

Figure 4. Blocking LDH does not affect the $[O_2]$ and [NADH] decreases. ***A***, Effect of LDH inhibition on lactate level in the extracellular solution (5 slices). Oxamate significantly inhibits lactate accumulation (the inhibition of LDH is even stronger than the reduction in lactate concentration shown in the graph, because lactate made before the oxamate was applied will not be removed by the oxamate). ***B***, Experimental protocol. Oxamate was added or not added during stage 2, and responses in ***E–G*** were expressed as a percentage of those in stage 1. ***C***, ***D***, Example traces showing the effect of 20 mM oxamate on the O_2 transient (***C***) and the NADH dip and overshoot produced by Schaffer collateral stimulation (***D***). ***E–G***, Mean data showing the effect of oxamate on the $[O_2]$ decrease (***E***), initial NADH fluorescence decrease (***F***), and late NADH fluorescence increase (***G***), normalized as in ***B***. Solutions contained 95% O_2.

In the presence of NBQX+AP5, to block postsynaptic currents and action potentials, the O_2 decrease was reduced to 32% of the value obtained in the absence of drugs, not significantly different to the reduction to 37% produced by NBQX+AP5 in 95% O_2 solution (Fig. 3*E*,*F*, statistics are given in the legend). Thus, the fraction of O_2 consumption that is on postsynaptic activity is approximately independent of O_2 level.

Effect of blocking lactate dehydrogenase

The astrocyte–neuron lactate shuttle hypothesis proposes that astrocytes carry out glycolysis and use LDH to convert the end product of glycolysis, pyruvate, into lactate, which is transferred to neurons where neuronal LDH converts it back to pyruvate to fuel neuronal oxidative phosphorylation (Fig. 1*H*). To test this hypothesis, we blocked LDH in astrocytes and neurons using 20 mM oxamate (the IC_{50} for block is 0.6–4.4 mM) (Wu et al., 2007). After 5 min, oxamate significantly reduced lactate levels in the bathing ACSF by 66 ± 7% ($p = 4.3 \times 10^{-4}$) (Fig. 4*A*), consistent with LDH being inhibited. According to the astrocyte–neuron lactate shuttle idea, this ought to reduce or abolish the O_2 decrease evoked by neuronal activity.

Blocking LDH also allows us to put limits on the relative importance of ATP production by oxidative phosphorylation and glycolysis. With interconversion of pyruvate and lactate blocked, if glycolytic ATP production were dominant, neuronal activity would produce a rise of NADH level, not a fall. Inspection of Figure 1*H* shows that, with LDH blocked, glycolysis generates 1 NADH molecule per ATP produced, and glycolysis followed by pyruvate entering the TCA cycle generates 2.5 NADH molecules per ATP produced, while oxidative phosphorylation consumes 10/26 or 0.38 NADH molecules per ATP produced. It follows that a rise of [NADH] is expected if, averaged over all the astrocytes and neurons imaged, the rate of production of ATP by glycolysis is >38% of the rate of ATP production by oxidative phosphorylation (or if the rate of ATP production by glycolysis followed by the TCA cycle is >38%/2.5 = 15% of that produced by oxidative phosphorylation). Thus, if neuronal activity evokes a fall of NADH fluorescence, it implies that oxidative phosphorylation generates >100% − 38% = 62% of the ATP powering the increase of neuronal activity (assuming that NADH generated in the cytoplasm rapidly equilibrates with mitochondrial NADH, the fluorescence of which may be enhanced by binding to proteins such as complex 1) (Blinova et al., 2008).

In the presence of oxamate, the resting level of $[O_2]$ and NADH fluorescence were unchanged (reduced by 1 ± 6%, $p = 0.83$, $N = 11$ and by 2 ± 2%, $p = 0.32$, $N = 13$, respectively). Furthermore, although oxamate reduced and slowed the field EPSC and population spike (see below, Effects of oxamate on field potentials), neuronal activity still evoked a decrease of $[O_2]$ and of NADH fluorescence (Fig. 4*C*,*D*), and the amplitudes of these decreases were not significantly different from when oxamate was absent ($p = 0.67$ and 0.53 respectively; Fig. 4*E*,*F*). However, oxamate significantly increased the late overshoot of NADH fluorescence ($p = 0.003$; Fig. 4*G*). This is expected because, when glycolysis is activated with a delay after stimulation (Kasischke et al., 2004) and produces pyruvate, block of the conversion of pyruvate to lactate results in less consumption of NADH (see Fig. 1*H*) and allows more pyruvate to enter the NADH-generating TCA cycle (which is being activated; Brennan et al., 2006).

Although oxamate is widely used as an inhibitor of LDH, it also inhibits pyruvate decarboxylase (an enzyme expressed in astrocytes and neurons, which converts pyruvate to oxaloacetate to top up the TCA cycle with molecules) and, when pyruvate levels are low, pyruvate uptake into mitochondria (Martin-Requero et al., 1986a,b). Furthermore it can produce a small inhibition of aspartate aminotransferase (Rej, 1979), a component of the malate–aspartate shuttle that transfers cytoplasmic NADH into mitochondria. These effects are unlikely to be significant in our preparation, since inhibition of pyruvate uptake, the TCA cycle, or NADH uptake in mitochondria would decrease

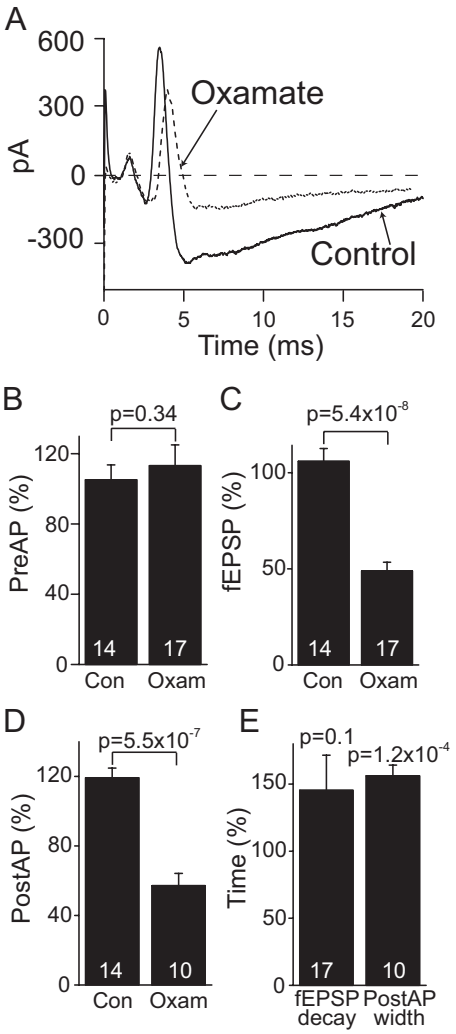

Figure 5. Effects of oxamate on field potentials. ***A***, Example traces showing the effect of 20 mM oxamate on the field potential produced by Schaffer collateral stimulation. ***B–D***, Effect of oxamate on the presynaptic action potential volley (preAP; ***B***), the fEPSP (***C***), and the postsynaptic population spike (postAP; ***D***). ***E***, Effect of oxamate on the half-maximum width of the population spike and on the fEPSP decay time constant. In control conditions, repeated stimulation had no effect on the kinetics of the population spike (half-maximum width, 110 ± 3% of that for first stimuli; $p = 0.12$; $n = 10$) or fEPSP (decay time constant, 114 ± 20%; $p = 0.47$; $n = 9$).

oxidative phosphorylation, yet in our experiments the activity-evoked $[O_2]$ decrease was unaffected by oxamate.

The fact that neuronal activity still evokes a fall of both $[O_2]$ and [NADH] with LDH blocked implies that the majority of the ATP (at least 62%, see above) that powers the stimulation-evoked neuronal activity is produced by oxidative phosphorylation. Furthermore, the lack of a change in the decrease of $[O_2]$ evoked by neuronal activity when LDH is blocked rules out a transfer of lactate from astrocytes to neurons as a substrate for oxidative phosphorylation to power neuronal activity, at least in the short term.

Effects of oxamate on field potentials

Despite its lack of effect on the $[O_2]$ and [NADH] decreases, oxamate approximately halved the amplitude of the field EPSP and the population spike (Fig. 5*A-D*). This is a greater reduction of the population spike than was reported previously by Schurr and Payne (2007). These data might suggest a decrease in charge entry generating the field EPSP and the postsynaptic action potentials, implying a decreased energy requirement in oxamate, which should be reflected in lower oxygen use (contrary to the experimental observations in Fig. 4*C*,*E*). However, oxamate also increased the duration of the population spike by a factor of ~1.6 ($p = 6.2 \times 10^{-5}$, Fig. 5*A*, *E*; modeling of the superimposed waveforms of the fEPSP and population spike showed that this was too large to result simply from the decrease of the underlying fEPSP) and increased the decay time of the fEPSP by a factor of ~1.5 (although this did not reach statistical significance; $p = 0.1$; Fig. 5*E*). This suggests that, for reasons unknown, oxamate decreased and prolonged the EPSC, leading to less synchronization of spike timing in different neurons. As a result, although the fEPSP and population spike are decreased and prolonged, the overall O_2 use does not change significantly.

Why oxamate alters the EPSC is unclear, but it does not appear to reflect a decrease of energy supply produced by a lack of substrate for oxidative phosphorylation, as applying pyruvate (1 mM) with oxamate did not prevent the changes in the fEPSP and population spike induced by oxamate (increased insignificantly by 3.0 ± 8.0%, $p = 0.71$, and 7 ± 15%, $p = 0.71$, respectively; $n = 8$, compared to oxamate alone). Oxygen usage was also unaffected by pyruvate supplementation (increased by 10 ± 7%, $p = 0.19$, $n = 9$, compared to oxamate alone). This suggests that either oxamate or the decrease in lactate concentration has a direct effect on the EPSC. Determining the mechanism of this effect is outside the scope of this study, but there may be contributions from a lactate-mediated decrease in prostaglandin uptake and rise of extracellular prostaglandin concentration (Chan et al., 2002; Gordon et al., 2008), which decreases EPSC amplitude but does not affect decay time (Koch et al., 2010) or from a promotion by lactate of hydroxyl radical formation (Ali et al., 2000) causing a peroxide-mediated increase of K_{ATP} channel activity (Avshalumov et al., 2005).

Modeling the relationship between the $[O_2]$ decrease and O_2 use

To use the effect of the drugs in Figure 2 to quantify the O_2 used on different subcellular mechanisms, we need to understand how the measured $[O_2]$ decrease relates to the increase of O_2 use evoked by neuronal activity. To establish this, we first estimated the resting O_2 usage in the slice, as in the study by Hall and Attwell (2008). The O_2 electrode was advanced through the slice to determine the profile of $[O_2]$ across the unstimulated slice. The results were not significantly different in the stratum pyramidale and stratum radiatum (repeated-measures ANOVA, $p = 0.26$, $N = 6$; Fig. 6*A*), and so were averaged (Fig. 6*B*). Next, these data were fitted with steady-state solutions (obtained using the *pdepe* function in Matlab) of the following diffusion equation:

$$D \cdot \delta^2 c/\delta x^2 = V_{max} \cdot c/(c + K_m) + \delta c/\delta t \qquad (1)$$

where x is distance into the slice, c is the concentration of O_2, D is its diffusion coefficient in brain at 37°C (1.54×10^{-9} m^2/s) (Ganfield et al., 1970), $K_m = 1$ μM is the EC_{50} for O_2 activating oxidative phosphorylation (Cooper, 2003), and V_{max} is the maximum rate of oxidative phosphorylation at saturating $[O_2]$. The boundary condition at the bottom of the slice ($x = 300$ μm, resting on the bath chamber) was assumed to be that $\delta c/\delta x = 0$. By fixing the value of $[O_2]$ at the slice surface at its measured value (387 ± 47 μM in 12 slices), and varying the value of V_{max}, it was found that the data were best fitted with $V_{max} = 0.7$ mM/min (Fig. 6*B*), about half the value found previously for acute cerebellar

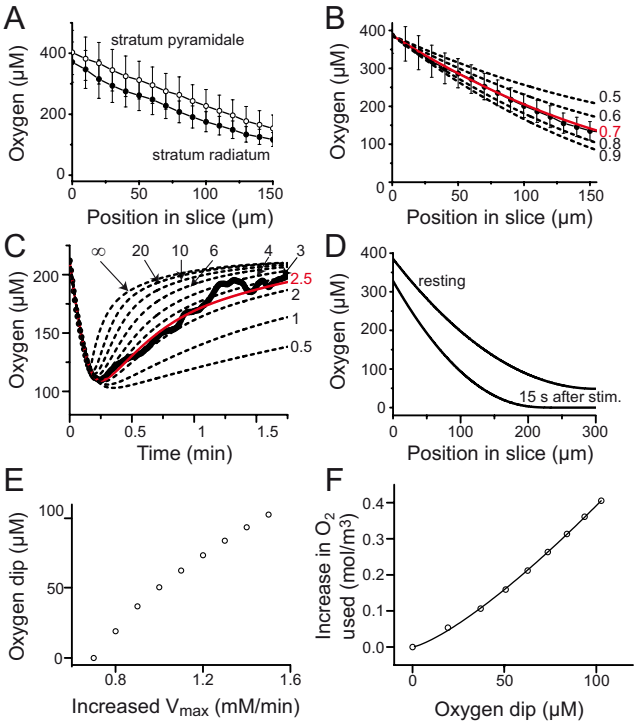

Figure 6. Modeling the O_2 consumption of the slice. ***A***, $[O_2]$ profile across the unstimulated slice in the stratum radiatum and stratum pyramidale ($N = 6$ slices). The slice surface is denoted position 0. ***B***, Mean of data in the two regions in ***A*** (circles), and theoretical fits for different assumed V_{max} values for O_2 consumption (given by each curve), constrained to have the value 387 μM at $x = 0$. The best fit (in red) is with $V_{max} = 0.7$ mM/min. ***C***, Fitting the $[O_2]$ decrease evoked by stimulation at a position 92 μm into the slice. Black circles are the mean control data in 95% O_2 from Figure 3*B*. Each smooth curve is the computed response to an increase of V_{max} from 0.7 to 1.5 mM/min, followed by a decay back to 0.7 mM/min with the rate constant (in min^{-1}) shown by each curve. The best fit (red) is with a rate constant of 2.5 min^{-1}, i.e., a time constant of 0.4 min or 24 s. ***D***, Predicted $[O_2]$ profiles across the slice in the resting state and at the peak of the O_2 dip following stimulation. ***E***, Predicted dependence of the amplitude of the $[O_2]$ transient on the underlying increase of the V_{max} for O_2 use. ***F***, Predicted relationship between the increase in O_2 consumed at the recording site and the size of the O_2 dip (the curve is O_2 consumption/mM $= 7.8 \times$ (oxygen dip/mM) $^{1.3}$).

slices but similar to the value found for cultured cerebellar slices (Hall and Attwell, 2008). Having established this value of V_{max}, we next estimated the thickness of the unstirred layer outside the slice, to allow us to compute changes of $[O_2]$ when V_{max} was raised by neuronal activity. This was done by solving Equation (1) both within the slice (with $V_{max} = 0.7$ mM/min) and outside the slice [with $V_{max} = 0$, D set to the free solution value of 2.74×10^{-9} m^2/s, at 35°C (van Stroe and Janssen, 1993), and the $[O_2]$ in the bulk solution set to 543 μM] (see Materials and Methods), and varying the unstirred layer thickness until the $[O_2]$ value measured at the surface of the slice (387 μM) was reproduced. The unstirred layer was thereby estimated to be 70 μm thick. In addition, from the profile of $[O_2]$ across the slice, it was possible to estimate how deep in the slice the O_2 electrode was positioned at the start of the experiments (estimated as 92 μm deep, similar to the intended depth of 100 μm).

With these parameters estimated, we next simulated how the $[O_2]$ profile across the slice was altered by Schaffer collateral stimulation. To mimic the effect of Na^+ entry stimulating ATP consumption by the Na^+/K^+-ATPase, and hence increasing O_2 use, we solved Equation (1) within the slice for a step increase of V_{max} (throughout the slice) from the 0.7 mM/min value derived above to a new higher value for 10 s, followed by an exponential decay back to 0.7 mM/min. In the unstirred layer outside the slice, Equation (1) was solved with $V_{max} = 0$. The initial values of $[O_2]$ across the slice were those calculated with V_{max} set to 0.7 mM/min and an unstirred layer thickness of 70 μm, as above. To reproduce the peak $[O_2]$ decrease seen in 95% O_2 in Figure 3*B* (at a distance 92 μm into the slice), it was necessary to increase V_{max} within the slice to 1.5 mM/min (i.e., an approximate doubling of the V_{max}), while to reproduce the decay time course of the O_2 transient, the time constant of decay of the V_{max} increase after stimulation had to be set to 24 s (a rate constant of 2.5 min^{-1}; Fig. 6*C*). The resulting profile of $[O_2]$ through the slice at the peak of the response is shown in Figure 6*D*. Although neuronal activity may not really produce an immediate and constant increase in the V_{max} for O_2 use throughout the stimulation period, this assumed time course for the increase in V_{max} during activity, and the subsequent exponential decrease, reproduced reasonably well the measured time course of the $[O_2]$ transient at a distance 92 μm into the slice. The calculated V_{max} of 1.5 mM/min is similar to the cerebral metabolic rate for oxygen measured *in vivo* in anesthetized rats (Ichord et al., 2001; Zhu et al., 2007) and about one-third of the value calculated from glucose usage in unanaesthetized rats (Sokoloff et al., 1977), implying that the neuronal activity that we are evoking is similar to that normally studied in anesthetized animals, but below the maximum level occurring in resting animals *in vivo*. This is probably not due to our use of P21 (rather than adult) rats, because the cerebral metabolic rate for oxygen is not significantly different at these two ages (Dahlquist and Persson, 1976). Presumably, therefore, we are not stimulating sufficient axons to generate activity matching that occurring *in vivo*.

With the response in control solution reasonably well reproduced, we then investigated the effect on the predicted $[O_2]$ transient of reducing the increase of V_{max}, to mimic the effect of reducing the activity-evoked increase of O_2 use with glutamate receptor blockers or Cd^{2+}. The aim was to assess how the amplitude of the $[O_2]$ transient was related to the change of V_{max} that generated it. For this analysis, we assumed that there was no change in the time constant with which the V_{max} decreased after activity. The resulting relationship between the amplitude of the $[O_2]$ decrease evoked by activity and the underlying increase of V_{max} was roughly linear, but with a decrease in slope at larger values of V_{max} (Fig. 6*E*). The nonlinearity in this relationship results from the fact that, in the depth of the slice, the predicted $[O_2]$ becomes comparable to the K_m for O_2 use by mitochondria (Fig. 6*D*), rendering Equation (1) nonlinear [unlike for $c \gg K_m$ when Eq. (1) becomes $D \cdot \delta^2 c/\delta x^2 - \delta c/\delta t = V_{max}$ so that changes of c are proportional to changes of V_{max}]. When we calculated the increased O_2 usage at the position of the O_2 electrode as (see Eq. 1) $V_{max}\, c/(c + K_m)$ and integrated over a 4 min period from when the 10 s stimulation started, this was found to vary approximately as the amplitude of the O_2 dip raised to the power 1.3 (Fig. 6*F*). Using this relationship, the changes in the amplitude of the O_2 dip measured in Figure 2 can be converted to relative O_2 usage on different mechanisms (see below, The fraction of O_2 use on the subcellular mechanisms mediating information processing).

A similar analysis showed that (in the absence of blocking drugs) the stimulation-evoked O_2 usage in 20% O_2 was 77% of that occurring in 95% O_2. This 23% decrease is approximately as expected, given the 38% decrease of fEPSP amplitude and 15% decrease of population spike amplitude seen in 20% O_2 (Fig. 3*A*). Thus, at an approximately physiological O_2 level, almost as much ATP is made by oxidative phosphorylation as occurs in 95% O_2.

Finally, we examined the sensitivity of the O_2 electrode for detecting O_2 usage at different spatial locations, by simulating in two dimensions (into the depth of the slice and across the slice

from the stratum radiatum and stratum lacunosum moleculare to the stratum oriens and alveus) the change in O_2 concentration that occurs. Starting from the steady-state solution to Equation 1 with V_{max} = 0.7 mM/min, we simulated the O_2 concentration change occurring when V_{max} was increased for 10 s to 1.5 mM/min, either solely in the stratum radiatum and stratum lacunosum moleculare (the combined width of which was measured as 258 μm in 6 slices) or solely in the stratum pyramidale, stratum oriens, and alveus (combined width measured as 184 μm). MathCad was used to solve by Euler's method the two-dimensional diffusion equation with O_2 consumption:

$$D \cdot (\delta^2 c/\delta x^2 + \delta^2 c/\delta y^2) = V_{max}(x,y,t) \cdot c/(c + K_m) + \delta c/\delta t \quad (2)$$

A distance step of 2 μm in each direction and a time step of 0.25 ms were used, after checking that 1 μm and 0.1 ms steps gave negligibly different results. At the location we placed the O_2 electrode (92 μm into the slice, at a distance 30 μm into the stratum radiatum) (see above), increasing V_{max} to 1.5 mM/min throughout the stratum radiatum and stratum lacunosum moleculare decreased $[O_2]$ by 61 μM, while increasing V_{max} to 1.5 mM/min throughout the alveus, stratum oriens, and stratum pyramidale decreased $[O_2]$ by 35 μM (i.e., 57% of 61 μM). Since the alveus/stratum oriens/stratum pyramidale is only 71% of the width of the stratum radiatum/stratum lacunosum moleculare (so the total increased O_2 use was only 71% of that assumed for the simulation when there was increased O_2 use in the stratum radiatum/stratum lacunosum moleculare), this means that the sensitivity to V_{max} increases in the alveus/stratum oriens/stratum pyramidale is 20% (1 − 57%/71%) less than for V_{max} changes in the stratum radiatum/stratum lacunosum moleculare. This might be thought to result in an underestimate of the O_2 use on postsynaptic action potentials, since in pyramidal cells these will use O_2 in the alveus, stratum oriens, and stratum pyramidale. However, the underestimate will be <20% (and is ignored in what follows), because some of the O_2 use on postsynaptic action potentials will occur in interneurons in the stratum radiatum.

To deduce the relationship between $[O_2]$ decrease and O_2 use in the experiments of Figure 2*H* using glutamate superfusion, simulations similar to those described for Figure 6*F* were performed for the longer period of O_2 usage evoked by glutamate superfusion, which predicted that O_2 usage would vary as the amplitude of the O_2 dip raised to the power 1.5.

The fraction of O_2 use on the subcellular mechanisms mediating information processing

Correcting the 63% reduction in the size of the stimulation-evoked $[O_2]$ transient that is produced by NBQX+AP5 in Figure 2*E*, for the nonlinearity of the relationship between $[O_2]$ dip and O_2 consumption that is shown in Figure 6*F*, we calculated that postsynaptic currents and postsynaptic action potentials are responsible for 72% of the O_2 usage. Similarly the 82% block of the O_2 transient produced by Cd^{2+}, when corrected for the nonlinearity of Figure 6*F*, implies that 89% of the O_2 is used on mechanisms that are blocked by Cd^{2+}. The difference between the 72% reduction of the $[O_2]$ usage produced by NBQX+AP5 and the 89% reduction produced by Cd^{2+} implies that events that are not triggered by activation of postsynaptic glutamate ionotropic receptors but are triggered by presynaptic Ca^{2+} entry (i.e., pumping out presynaptic Ca^{2+}, vesicle release and refilling, actions of mGluRs, and transmitter uptake) consume 17% of the O_2. The difference between the 89% reduction of $[O_2]$ usage by Cd^{2+} and the complete block produced by TTX implies that 11% of the O_2 usage is on presynaptic action potentials. This division of O_2 usage is shown in Figure 7*A*.

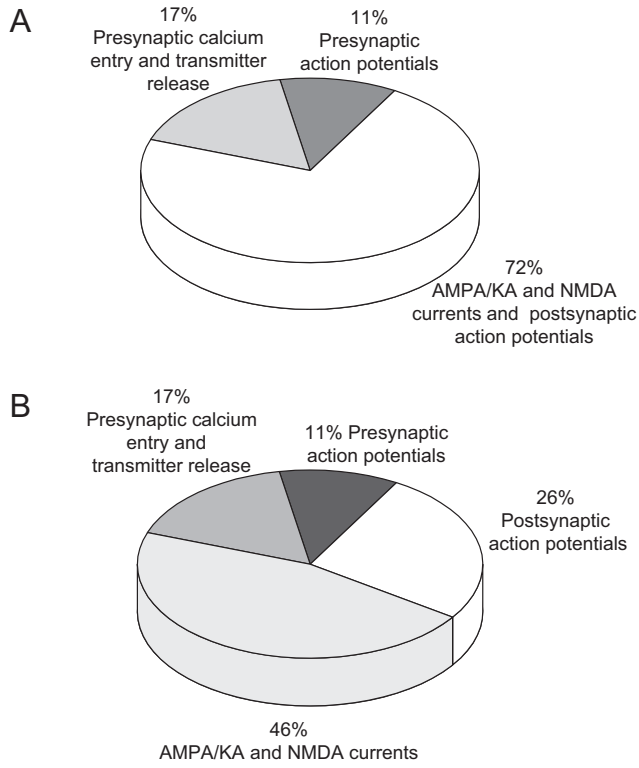

Figure 7. The distribution of O_2 use across different subcellular processes. ***A***, The O_2 use on AMPA/KA and NMDA receptor currents and postsynaptic action potentials (blocked by NBQX+AP5); on presynaptic Ca^{2+} entry, vesicle release and refilling, mGluR activity, and transmitter uptake (blocked by Cd^{2+} but not by NBQX); and on presynaptic action potentials (blocked by TTX but not by Cd^{2+}). ***B***, The O_2 use on different subcellular mechanisms derived from ***A*** by using the analysis of O_2 use on postsynaptic glutamate-gated currents and action potentials derived from experiments applying glutamate in Figure 2*I*. Activity-induced ATP use on mGluRs and astrocytes are ignored, but were estimated by Attwell and Laughlin (2001) to be ~2% and <7% of that in neurons, respectively.

With the split of energy use between presynaptic and postsynaptic mechanisms given above, we can use the data in Figure 2*I* to estimate how the O_2 consumption on postsynaptic mechanisms is divided between glutamate-gated ion channels and action potentials, if we assume that glutamate-evoked energy use on mGluRs and in astrocytes is small [Attwell and Laughlin (2001) estimated that, for each vesicle of glutamate released, the ATP use on mGluRs was only 2.2% of that on ionotropic glutamate receptors, and the ATP use in astrocytes was only 6.8% of that in neurons or less if ATP use on action potentials was included]. To do this, we assume that the dependence of action potential firing rate on mean glutamate-gated current is the same when action potentials are evoked by superfusing glutamate (as in Fig. 2*I*) and by activating the Schaffer collateral input (as in Fig. 2*E*), so that the relative magnitudes of the ion influxes through glutamate-gated channels and through voltage-gated Na^+ channels are the same in both situations. With this assumption, the 29% reduction of the O_2 dip seen in Figure 2*I* was transformed through a relationship like that in Figure 6*F* (see above). This transformation predicted that the O_2 use attributed to postsynaptic mechanisms above is split between postsynaptic glutamate-gated currents and postsynaptic action potentials in a ratio of 64 to 36%, implying that 46% (i.e., 72% × 0.64) of the O_2 use evoked by Schaffer collateral stimulation is on postsynaptic

currents, and 26% (72% × 0.36) is on postsynaptic action potentials. Combining these O_2 usages, with those for presynaptic action potentials and nonpostsynaptic events downstream of presynaptic Ca^{2+} entry in Figure 7*A*, gives the division of O_2 use shown in Figure 7*B*.

NADH usage

Knowing the amount of oxygen used during Schaffer collateral stimulation allows us to calculate the NADH turnover that must be occurring. From the curve fit to Figure 6*F* and the mean oxygen dip of 118 μM (Fig. 1), 0.485 mM O_2 can be calculated to be consumed following Schaffer collateral stimulation. Ten NADH molecules are used for each 6 O_2 molecules consumed (Fig. 1*H*), implying a usage of 0.808 mM NADH. Importantly, the resting level of NADH in hippocampus is only 0.057 μmol/g tissue (Klaidman et al., 1995), or 60 μM assuming a density of 1.05 g/ml. Using this resting NADH concentration, the measured 1.4% decrease of [NADH] (Fig. 1*F*) implies that [NADH] decreases by only 0.84 μM, underrepresenting the absolute usage of NADH by three orders of magnitude. High rates of both NADH production and consumption must, therefore, be occurring during the NADH dip period and, since oxygen is still being used (Fig. 3*D*), during the overshoot. As the NADH dip and overshoot poorly reflect the actual amounts of NADH used and generated, they cannot be used to quantify the amount of oxidative phosphorylation or glycolysis occurring. For this reason, we limit our interpretation of the NADH changes to arguing that the existence of a dip means that there is a larger relative contribution of oxidative phosphorylation than glycolysis to ATP production following neuronal stimulation (see above).

Discussion

Our data lead to three major conclusions for the powering of neuronal activity. First, the majority of the ATP powering increases of neuronal activity is produced by oxidative phosphorylation. Second, the main mechanisms contributing to information processing, i.e., presynaptic action potentials, transmitter release, postsynaptic currents, and postsynaptic action potentials, are all powered by ATP generated from oxidative phosphorylation. Third, the simplest version of the astrocyte–neuron lactate shuttle hypothesis, in which neuronal activity initially triggers ATP generation by glycolysis in astrocytes which then release lactate to rapidly power neuronal oxidative phosphorylation, is not consistent with our data.

The majority of ATP is generated by oxidative phosphorylation

Neuronal activity evoked by stimulating the Schaffer collaterals generated an initial decrease in both extracellular [O_2] and intracellular [NADH] (Fig. 1). These decreases were also seen when a physiological oxygen level was produced in the slice by superfusion with solution gassed with 20% oxygen (Fig. 3), and they still occurred when lactate dehydrogenase was blocked with oxamate (Fig. 4). The fact that a decrease of [NADH] is seen, averaged over the neurons and astrocytes in the slice, with lactate dehydrogenase blocked to prevent interconversion of pyruvate and lactate, implies that at least 62% of the increase in ATP production which occurs in the slice to power the increase in neuronal activity is generated by oxidative phosphorylation (see Results).

As reviewed in the introduction, the association of glycolytic enzymes with ion pumps, the apparently larger fractional increase of glucose uptake than of oxygen uptake in response to neuronal activity (Fox et al., 1988) [but see the study by Madsen et al. (1999), who found a less significant decrease of the O_2: glucose utilization ratio], and the notion that neurons regulate their energy supply by initially increasing glycolysis in astrocytes, all suggested that neuronal activity was initially powered by glycolysis. Our data show, on the contrary, that oxidative phosphorylation is responsible for most of the increase in ATP production. In a methodologically very different approach, magnetic resonance imaging and spectroscopy have recently suggested a similar conclusion (Lin et al., 2010).

The change of O_2 concentration evoked by 10 s of 20 Hz stimulation of the Schaffer collaterals could be predicted if the rate of O_2 consumption approximately doubled at the start of stimulation and decayed exponentially after the stimulation with a time constant of 24 s (Fig. 6). Although we assumed an immediate rise in O_2 consumption in our model, in reality it is likely that the rise is slower (set by the rate of rise of $[Na^+]_i$ and $[K^+]_o$, which stimulate sodium pump activity), and that the kinetics of the fall of [O_2] are set by diffusive equilibration with the bulk solution and are not critically dependent on the rate at which O_2 usage turns on. The recovery of [O_2] use after stimulation is much slower than is predicted if metabolic demand were removed immediately when the stimulation stopped (Fig. 6*C*), and presumably the 24 s decay of O_2 use that we derived for 95% O_2 reflects the time needed for the sodium pump to restore the ion gradients across the cell membranes. In 20% O_2, the decay of O_2 use was greatly prolonged (Fig. 3*B*), implying that the local O_2 level in the brain will influence the time scale on which neurons can reinstate their ion gradients after activity.

After the initial decrease of [O_2] and [NADH], there was an increase of [NADH] above its prestimulus level, which may reflect increased NADH production either by glycolysis or by an increased activity of the TCA cycle. The [NADH] overshoot overlaps in time with the prolonged decrease in [O_2] evoked by stimulation (Fig. 3*D*) and so occurs at a time when oxidative phosphorylation is increased.

The distribution of O_2 consumption on different subcellular mechanisms

Using pharmacological agents to isolate different subcellular mechanisms contributing to neuronal activity, we demonstrated that presynaptic activity, transmitter release and recycling, and postsynaptic activity are all powered at least partly by oxidative phosphorylation (Fig. 2). Using the response to superfused glutamate, in the presence and absence of TTX, to separate energy use on postsynaptic glutamate-gated currents and on action potentials, we estimate that presynaptic action potentials consume ~11%; presynaptic Ca^{2+} entry, transmitter release/recycling, and mGluR activity consume ~17%; postsynaptic currents use ~46%; and postsynaptic action potentials consume ~26% of the O_2 (Fig. 7*B*), so presynaptic and postsynaptic action potentials together use 37% of the O_2.

Thus, the present findings provide evidence against the hypotheses that most energy is used presynaptically (Jueptner and Weiller, 1995) or that action potential propagation operates mainly anaerobically (Lecoq et al., 2009). On the other hand, they support findings showing that a large fraction of energy consumption is postsynaptically driven (Attwell and Laughlin, 2001; Offenhauser et al., 2005).

The energy budget of Attwell and Laughlin (2001) for rat cortex predicts the energy used on different components of neuronal signaling. From their Figure 3*A*, ignoring ATP used on the resting potential and reducing the action potential energy use by a factor of 3.08 to compensate for the fact that mammalian neurons use 3.08-fold less energy (per membrane area) on action potentials

than do the squid action potentials that the Attwell and Laughlin (2001) budget was based on (Alle et al., 2009), action potentials are expected to use 28%, presynaptic Ca^{2+} entry, transmitter release/recycling, and mGluRs 11%, and postsynaptic currents 61% of the stimulation-evoked ATP consumption. This is in reasonable agreement with Figure 7*B*, considering that we are studying hippocampus and not cortex, and that the relative contributions of the different mechanisms may vary with stimulus frequency (e.g., due to AMPA receptor desensitization or NMDA receptors experiencing less Mg^{2+} block during high-frequency stimulation).

Implications for the astrocyte–neuron lactate shuttle hypothesis

The astrocyte–neuron lactate shuttle hypothesis assumes that astrocytes convert glycolytically derived pyruvate to lactate using lactate dehydrogenase, before exporting it to neurons where it is converted back to pyruvate, again by lactate dehydrogenase, and then enters the TCA cycle as fuel for oxidative phosphorylation (Fig. 1*H*). On this basis, one might expect blocking lactate dehydrogenase to abolish or reduce the increase in O_2 consumption evoked by neuronal activity. We found, however, that the LDH blocker oxamate had no effect on the initial decrease in $[O_2]$ or [NADH] that is evoked by Schaffer collateral stimulation (Fig. 4). We conclude that the increase in oxidative phosphorylation that generates ATP to power an increase of neuronal activity does not require lactate transfer from astrocytes.

It is worth highlighting that, at P21, rats express their highest levels of the monocarboxylate transporter responsible for transporting lactate into neurons (MCT2), with expression decreasing thereafter (Prins, 2008), and increased MCT2 expression is proposed to lead to increased lactate shuttle activity (Pellerin and Magistretti, 2011). If neuronal energy metabolism does not depend on lactate transfer at P21, therefore, it is unlikely to contribute at older ages, when MCT2 expression is lower.

Apparently contradicting our findings, Schurr and Payne (2007) and Schurr and Gozal (2011) found that inhibiting LDH with malonate or oxamate decreased neuronal function when hippocampal slices were maintained in glucose or lactate, but that neuronal function could be preserved by superfusing pyruvate, supporting the idea of a lactate shuttle. However, effects of malonate and oxamate on neuronal function were only seen after 30–45 min or after excitotoxic challenge. Furthermore, and crucially, oxidative phosphorylation was not monitored by recording oxygen level, so the interpretation of the data presented in terms of altered ATP production by mitochondria is not secure. We suggest that, while lactate may be important for long-term functioning of the slice, it is not required for the short-term increase in oxidative phosphorylation that occurs after an increase in neuronal activity. This interpretation is consistent with a recent review (Mangia et al., 2011) of contradictory modeling studies that disagreed over whether lactate passes from astrocytes to neurons or from neurons to astrocytes. Mangia et al. (2011) concluded that, whichever way lactate moves, its contribution to oxidative phosphorylation is small (Dienel and Cruz, 2008). An export of lactate from astrocytes to neurons was suggested previously to be essential for hippocampal synaptic plasticity (Suzuki et al., 2011). Our data suggest that this effect may be mediated by lactate functioning as a signaling molecule (Song and Routh, 2005; Shimizu et al., 2007; Bezzi and Volterra, 2011), rather than as a metabolic substrate.

References

Akgören N, Fabricius M, Lauritzen M (1994) Importance of nitric oxide for local increases of blood flow in rat cerebellar cortex during electrical stimulation. Proc Natl Acad Sci U S A 91:5903–5907.

Ali MA, Yasui F, Matsugo S, Konishi T (2000) The lactate-dependent enhancement of hydroxyl radical generation by the Fenton reaction. Free Radic Res 32:429–438.

Alle H, Roth A, Geiger JR (2009) Energy-efficient action potentials in hippocampal mossy fibers. Science 325:1405–1408.

Amato A, Ballerini L, Attwell D (1994) Intracellular pH changes produced by glutamate uptake in rat hippocampal slices. J Neurophysiol 72:1686–1696.

Attwell D, Laughlin SB (2001) An energy budget for signaling in the grey matter of the brain. J Cereb Blood Flow Metab 21:1133–1145.

Aubin JE (1979) Autofluorescence of viable cultured mammalian cells. J Histochem Cytochem 27:36–43.

Avshalumov MV, Chen BT, Koós T, Tepper JM, Rice ME (2005) Endogenous hydrogen peroxide regulates the excitability of midbrain dopamine neurons via ATP-sensitive potassium channels. J Neurosci 25:4222–4231.

Barros LF, Deitmer JW (2010) Glucose and lactate supply to the synapse. Brain Res Rev 63:149–159.

Bezzi P, Volterra A (2011) Astrocytes: powering memory. Cell 144:644–645.

Blinova K, Levine RL, Boja ES, Griffiths GL, Shi ZD, Ruddy B, Balaban RS (2008) Mitochondrial NADH fluorescence is enhanced by complex I binding. Biochemistry 47:9636–9645.

Brazitikos PD, Pournaras CJ, Munoz JL, Tsacopoulos M (1993) Microinjection of L-lactate in the preretinal vitreous induces segmental vasodilation in the inner retina of miniature pigs. Invest Ophthalmol Vis Sci 34:1744–1752.

Brennan AM, Connor JA, Shuttleworth CW (2006) NAD(P)H fluorescence transients after synaptic activity in brain slices: predominant role of mitochondrial function. J Cereb Blood Flow Metab 26:1389–1406.

Caesar K, Thomsen K, Lauritzen M (2003) Dissociation of spikes, synaptic activity, and activity-dependent increments in rat cerebellar blood flow by tonic synaptic inhibition. Proc Natl Acad Sci U S A 100:16000–16005.

Chan BS, Endo S, Kanai N, Schuster VL (2002) Identification of lactate as a driving force for prostanoid transport by prostaglandin transporter PGT. Am J Physiol Renal Physiol 282:F1097–F1102.

Chance B, Williams GR (1955) Respiratory enzymes in oxidative phosphorylation. III. The steady state. J Biol Chem 217:409–427.

Contreras L, Satrústegui J (2009) Calcium signaling in brain mitochondria: interplay of malate aspartate NADH shuttle and calcium uniporter/mitochondrial dehydrogenase pathways. J Biol Chem 284:7091–7099.

Cooper CE (2003) Competitive, reversible, physiological? Inhibition of mitochondrial cytochrome oxidase by nitric oxide. IUBMB Life 55:591–597.

Dahlquist G, Persson B (1976) The rate of cerebral utilization of glucose, ketone bodies and oxygen: a comparative *in vivo* study of infant and adult rats. Pediat Res 10:910–917.

Dienel GA, Cruz NF (2008) Imaging brain activation: simple pictures of complex biology. Ann N Y Acad Sci 1147:139–170.

Dings J, Meixensberger J, Jäger A, Roosen K (1998) Clinical experience with 118 brain tissue oxygen partial pressure catheter probes. Neurosurgery 43:1082–1095.

Dubinsky WP, Mayorga-Wark O, Schultz SG (1998) Colocalization of glycolytic enzyme activity and KATP channels in basolateral membrane of *Necturus* enterocytes. Am J Physiol 275:C1653–C1659.

Duchen MR (1992) Ca^{2+}-dependent changes in the mitochondrial energetics in single dissociated mouse sensory neurons. Biochem J 283:41–50.

Fox PT, Raichle ME, Mintun MA, Dence C (1988) Nonoxidative glucose consumption during focal physiologic neural activation. Science 241:462–464.

Ganfield RA, Nair P, Whalen WJ (1970) Mass transfer, storage, and utilization of O_2 in cat cerebral cortex. Am J Physiol 219:814–821.

Gellerich FN, Gizatullina Z, Arandarcikaite O, Jerzembek D, Vielhaber S, Seppet E, Striggow F (2009) Extramitochondrial Ca^{2+} in the nanomolar range regulates glutamate-dependent oxidative phosphorylation on demand. PLoS One 4:e8181.

Gellerich FN, Gizatullina Z, Trumbeckaite S, Nguyen HP, Pallas T, Arandarcikaite O, Vielhaber S, Seppet E, Striggow F (2010) The regulation of OXPHOS by extramitochondrial calcium. Biochim Biophys Acta 1797:1018–1027.

Gjedde A (2005) The pathways of oxygen in brain. I. Delivery and metabolism of oxygen. Adv Exp Med Biol 566:269–275.
Gordon GR, Choi HB, Rungta RL, Ellis-Davies GC, MacVicar BA (2008) Brain metabolism dictates the polarity of astrocyte control over arterioles. Nature 456:745–749.
Gunter TE, Yule DI, Gunter KK, Eliseev RA, Salter JD (2004) Calcium and mitochondria. FEBS Lett 567:96–102.
Hall CN, Attwell D (2008) Assessing the physiological concentration and targets of nitric oxide in brain tissue. J Physiol 586:3597–3615.
Hyder F, Patel AB, Gjedde A, Rothman DL, Behar KL, Shulman RG (2006) Neuronal-glial glucose oxidation and glutamatergic-GABAergic function. J Cereb Blood Flow Metab 26:865–877.
Ichord RN, Johnston MV, Traystman RJ (2001) MK801 decreases glutamate release and oxidative metabolism during hypoglycemic coma in piglets. Brain Res Dev Brain Res 128:139–148.
Jang IS, Ito Y, Akaike N (2005) Feed forward facilitation of glutamate release by presynaptic $GABA_A$ receptors. Neuroscience 135:737–748.
Jueptner M, Weiller C (1995) Does measurement of regional cerebral blood flow reflect synaptic activity? Implications for PET and fMRI. Neuroimage 2:148–156.
Kasischke KA, Vishwasrao HD, Fisher PJ, Zipfel WR, Webb WW (2004) Neural activity triggers neuronal oxidative metabolism followed by astrocytic glycolysis. Science 305:99–103.
Kety SS (1957) The general metabolism of the brain *in vivo*. In: Metabolism of the nervous system (Richter D, ed), pp 221–237. London: Pergamon.
Klaidman LK, Leung AC, Adams JD (1995) High-performance liquid chromatography analysis of oxidized and reduced pyridine dinucleotides in specific brain regions. Analyt Biochem 228:312–317.
Knull HR (1978) Association of glycolytic enzymes with particulate fractions from nerve endings. Biochim Biophys Acta 522:1–9.
Koch H, Huh SE, Elsen FP, Carroll MS, Hodge RD, Bedogni F, Turner MS, Hevner RF, Ramirez JM (2010) Prostaglandin E_2-induced synaptic plasticity in neocortical networks of organotypic slice cultures. J Neurosci 30:11678–11687.
Lecoq J, Tiret P, Najac M, Shepherd GM, Greer CA, Charpak S (2009) Odor-evoked oxygen consumption by action potential and synaptic transmission in the olfactory bulb. J Neurosci 29:1424–1433.
Leutgeb JK, Leutgeb S, Moser MB, Moser EI (2007) Pattern separation in the dentate gyrus and CA3 of the hippocampus. Science 315:961–966.
Li J, Iadecola C (1994) Nitric oxide and adenosine mediate vasodilation during functional activation in cerebellar cortex. Neuropharmacol 33:1453–1461.
Lin AL, Fox PT, Hardies J, Duong TQ, Gao JH (2010) Nonlinear coupling between cerebral blood flow, oxygen consumption, and ATP production in human visual cortex. Proc Natl Acad Sci U S A 107:8446–8451.
Lipton P, Robacker K (1983) Glycolysis and brain function: $[K+]_o$ stimulation of protein synthesis and K^+ uptake require glycolysis. Fed Proc 42:2875–2880.
Lu M, Holliday LS, Zhang L, Dunn WA Jr, Gluck SL (2001) Interaction between aldolase and vacuolar H^+-ATPase: evidence for direct coupling of glycolysis to the ATP-hydrolyzing proton pump. J Biol Chem 276: 30407–30413.
Madsen PL, Cruz NF, Sokoloff L, Dienel GA (1999) Cerebral oxygen/glucose ratio is low during sensory stimulation and rises above normal during recovery: excess glucose consumption during stimulation is not accounted for by lactate efflux from or accumulation in brain tissue. J Cereb Blood Flow Metab 19:393–400.
Magistretti PJ, Pellerin L, Rothman DL, Shulman RG (1999) Energy on demand. Science 283:496–497.
Malonek D, Grinvald A (1996) Interactions between electrical activity and cortical microcirculation revealed by imaging spectroscopy: implications for functional brain mapping. Science 272:551–554.
Mangia S, DiNuzzo M, Giove F, Carruthers A, Simpson IA, Vannucci SJ (2011) Response to 'comment on recent modeling studies of astrocyte-neuron metabolic interactions': much ado about nothing. J Cereb Blood Flow Metab 31:1346–1353.
Martin-Requero A, Ayuso MS, Parrilla R (1986a) Interaction of oxamate with the gluconeogenic pathway in liver. Arch Biochem Biophys 246:114–127.
Martin-Requero A, Ayuso MS, Parrilla R (1986b) Rate-limiting steps for hepatic gluconeogenesis. Mechanism of oxamate inhibition of mitochondrial pyruvate metabolism. J Biol Chem 261:13973–13978.
Mathiesen C, Caesar K, Thomsen K, Hoogland TM, Witgen BM, Brazhe A, Lauritzen M (2011) Activity-dependent increases in local oxygen consumption correlate with postsynaptic currents in the mouse cerebellum *in vivo*. J Neurosci 31:18327–18337.
Mercer RW, Dunham PB (1981) Membrane-bound ATP fuels the Na/K pump. Studies on membrane-bound glycolytic enzymes on inside-out vesicles from human red cell membranes. J Gen Physiol 78:547–568.
Offenhauser N, Thomsen K, Caesar K, Lauritzen M (2005) Activity induced tissue oxygenation changes in rat cerebellar cortex: interplay of postsynaptic activation and blood flow. J Physiol 565:279–294.
Ogawa S, Lee TM, Barrere B (1993) The sensitivity of magnetic resonance image signals of a rat brain to changes in the cerebral venous blood oxygenation. Magn Reson Med 29:205–210.
Paul RJ, Bauer M, Pease W (1979) Vascular smooth muscle: aerobic glycolysis linked to sodium and potassium transport processes. Science 206: 1414–1416.
Paul RJ, Hardin CD, Raeymaekers L, Wuytack F, Casteels R (1989) Preferential support of Ca2+ uptake in smooth muscle plasma membrane vesicles by an endogenous glycolytic cascade. FASEB J 3:2298–2301.
Pellerin L, Bouzier-Sore AK, Aubert A, Serres S, Merle M, Costalat R, Magistretti PJ (2007) Activity-dependent regulation of energy metabolism by astrocytes: an update. Glia 55:1251–1262.
Pellerin L, Magistretti PJ (1994) Glutamate uptake into astrocytes stimulates aerobic glycolysis: a mechanism coupling neuronal activity to glucose utilization. Proc Natl Acad Sci U S A 91:10625–10629.
Pellerin L, Magistretti PJ (2011) Sweet sixteen for ANLS. J Cereb Blood Flow Metab. Advance online publication. Retrieved October 26, 2011. doi: 10.1038/jcbfm.2011.149.
Prins ML (2008) Cerebral metabolic adaptation and ketone metabolism after brain injury. J Cereb Blood Flow Metab 28:1–16.
Rej R (1979) Measurement of aspartate aminotransferase activity: effects of oxamate. Clin Chem 25:555–559.
Schurr A, Gozal E (2011) Aerobic production and utilization of lactate satisfy increased energy demands upon neuronal activation in hippocampal slices and provide neuroprotection against oxidative stress. Front Pharmacol 2:96.
Schurr A, Payne RS (2007) Lactate, not pyruvate, is neuronal aerobic glycolysis end product: an in vitro electrophysiological study. Neuroscience 147:613–619.
Shimizu H, Watanabe E, Hiyama TY, Nagakura A, Fujikawa A, Okado H, Yanagawa Y, Obata K, Noda M (2007) Glial Na_x channels control lactate signaling to neurons for brain $[Na^+]$ sensing. Neuron 54:59–72.
Sokoloff L (1960) The metabolism of the central nervous system *in vivo*. In: Handbook of Physiology, Section I, Neurophysiology, Vol. 3 (Field J, Magoun HW, Hall VE, eds), pp 1843–1864. Washington D.C.: American Physiological Society.
Sokoloff L, Reivich M, Kennedy C, Des Rosiers MH, Patlak CS, Pettigrew KD, Sakurada O, Shinohara M (1977) The $[^{14}C]$deoxyglucose method for the measurement of local cerebral glucose utilization: theory, procedure, and normal values in the conscious and anesthetized albino rat. J Neurochem 28:897–916.
Song Z, Routh VH (2005) Differential effects of glucose and lactate on glucosensing neurons in the ventromedial hypothalamic nucleus. Diabetes 54:15–22.
Suzuki A, Stern SA, Bozdagi O, Huntley GW, Walker RH, Magistretti PJ, Alberini CM (2011) Astrocyte-neuron lactate transport is required for long-term memory formation. Cell 144:810–823.
Territo PR, Mootha VK, French SA, Balaban RS (2000) Ca^{2+} activation of heart mitochondrial oxidative phosphorylation: role of the F_oF_1-ATPase. Am J Physiol Cell Physiol 278:C423–C435.
Thompson JK, Peterson MR, Freeman RD (2003) Single-neuron activity and tissue oxygenation in the cerebral cortex. Science 299:1070–1072.
van Stroe AJ, Janssen LJJ (1993) Determination of the diffusion coefficient of oxygen in sodium chloride solutions with a transient pulse technique. Analyt Chim Acta 279:213–219.
Wu M, Neilson A, Swift AL, Moran R, Tamagnine J, Parslow D, Armistead S, Lemire K, Orrell J, Teich J, Chomicz S, Ferrick DA (2007) Multiparameter metabolic analysis reveals a close link between attenuated mitochondrial bioenergetic function and enhanced glycolysis dependency in human tumor cells. Am J Physiol 292:C126–C136.
Zhu XH, Zhang Y, Zhang N, Ugurbil K, Chen W (2007) Noninvasive and three-dimensional imaging of $CMRO_2$ in rats at 9.4 T: reproducibility test and normothermia/ hypothermia comparison study. J Cereb Blood Flow Metab 27:1225–1234.